



CHORUS

This is the accepted manuscript made available via CHORUS. The article has been published as:

Spin-dependent electronic processes and long-lived spin coherence of deep-level trap sites in CdS nanocrystals

K. J. van Schooten, J. Huang, D. V. Talapin, C. Boehme, and J. M. Lupton

Phys. Rev. B **87**, 125412 — Published 13 March 2013

DOI: [10.1103/PhysRevB.87.125412](https://doi.org/10.1103/PhysRevB.87.125412)

Spin-dependent electronic processes and long lived spin-coherence of deep-level trap sites in CdS nanocrystals

K. J. van Schooten¹, J. Huang², D. V. Talapin^{2,3}, C. Boehme^{1,*} and J. M. Lupton^{1,4,*}

¹Department of Physics and Astronomy, University of Utah, 115 South 1400 East, Salt Lake City, Utah 84112, USA

²Department of Chemistry, University of Chicago, Chicago, Illinois 60637, USA

³Center for Nanoscale Materials, Argonne National Laboratory, Argonne, Illinois 60439, USA

⁴Institut für Experimentelle und Angewandte Physik, Universität Regensburg, D-93040 Regensburg, Germany

Carrier trapping in colloidal nanocrystals represents a major energy loss mechanism for excitonic states crucial to devices. Surprisingly little is known about the influence of the spin degree of freedom on the nature of these intrinsic trap centers or the types of coupling that these states experience. Here, a pulsed microwave optically-detected magnetic resonance (pODMR) study is presented that aims to probe the interaction pathways existing between shallow band-edge trap states and the deep-level emissive chemical defect states responsible for the broad, low-energy emission common to CdS nanocrystals. Due to long spin-coherence times (T_2) of these states, Rabi flopping detected in the luminescence under magnetic resonance provides access to information regarding the modes of coupling of shallow-trapped electron-hole pairs, both of isolated species and of those in proximity to the emissive defect. Corresponding optically detected spin-echo experiments expose an extraordinarily long intrinsic spin coherence time ($T_2 \approx 1.6 \mu\text{s}$) for colloidal nanocrystals, and an electron spin-echo envelope modulation indicative of local spin interactions. This effect provides opportunities for gaining the detailed chemical and structural information needed in order to eliminate energy loss mechanisms during the synthetic process.

*Corresponding authors. Email: john.lupton@physik.uni-regensburg.de ; boehme@physics.utah.edu

Substantial advances in the fundamental understanding of electronic states characterizing colloidal nanocrystals have been made in recent years, which have facilitated the development of novel and exciting device concepts based on this unique material system. These proposed technologies range from next-but-one-generation photovoltaics [1] over multi-color lasers [2] to inkjet-printed LED displays on flexible substrates [3]. Plaguing the further development of such devices has been the existence of charge trap states and chemical defects [4], [5], which arise naturally during the conventional synthesis process, but provide strong alternative decay pathways [6] for the desired excitonic and multi-excitonic excited states. The origin of these deleterious states has been attributed to surface dangling bonds arising from ligand loss [7], incorrectly bonded passivation ligands [8], as well as crystalline defects such as vacancies and adatoms [9], [10]. The effects of such states are readily detected through observables of conventional optical probes, such as by monitoring single particle luminescence intermittency [11–13] (i.e. “blinking”) and the broad, sub-band gap chemical defect emission [9,10,14] commonly observed independent of synthesis technique or matrix employed [9,15–17]. In fact, several fairly complex models have been formulated in order to describe the complexity witnessed in photoluminescence (PL) blinking [18,19] and decay dynamics [20–22], which generally depend on certain assumptions about the population and decay pathways of both band-edge and trap or defect states, and their respective interactions. Even though these models go to great lengths in order to describe the complex dynamics observed experimentally, they are often not detailed enough, since they normally do not account for the existence of multiple trap species, and the possibility of both electron and hole traps, which has recently been confirmed for at least one type of nanocrystal [23]. In general, very little is actually known about the chemical nature of these trap states or the types of interactions

carriers experience within them since they are difficult to address directly using optical techniques alone. Spin resonance methods, on the other hand, are uniquely suited as a probe for such states and have historically proven to be a powerful tool in elucidating the chemical and electronic nature of charge traps and structural defects in a wide range of semiconductor systems [24–26].

Here, we use pulsed optically-detected magnetic resonance (pODMR) in order to directly probe trapped carriers which are associated with both band-edge as well as deep-level chemical defect emission in wurtzite CdS nanocrystalline nanorods with homogeneous dimensions of approximately 6 nm by 30 nm (the synthesis details follow those of Ref. 17). It is well known that band-edge excitons can be “shelved” in band-edge trap states, leading to delayed PL at times much longer than the exciton lifetime [21]. We observe that these charge traps, which shelve the primary exciton [27], are capable of interacting with both band-edge excitonic states as well as with the emissive deep-level chemical defect. The former leads to emission from the quantum-confined exciton, whereas the latter case of spectrally-shifted emission gives rise to a modification of the spin resonance properties of the band-edge trap states. We explore the trap states which are more directly associated with the chemical defect emission process, demonstrating that these are spatially highly localized with substantial dipolar coupling between carrier spins, as is most clearly manifested in the appearance of a half-field resonance. These states can be utilized as a probe of the local environment through electron-spin echo envelope modulation (ESEEM), which becomes possible due to the extraordinarily long spin coherence time of carriers in this state ($T_2 \approx 1.6 \mu\text{s}$) at 3.5 K.

The pODMR spin-resonance technique is limited by a carrier’s lifetime within a particular state relative to the timescale of spin-mixing induced by a resonant microwave pulse

(~10 ns). In this case, the trapping lifetime must be long and trapped carriers must directly feed one of the two primary emission channels, our observables for this material system: that is, the excitonic band-edge emission at 464 nm, and the deep-level chemical defect emission at ~635 nm [9]. Optical investigations of this defect emission in CdS nanocrystals, both with [10] and without [9] surface charge modification, have concluded that the emissive center is strongly related to surface S^{2-} and Cd^{2+} ion vacancies which serve as electron and hole traps, respectively, and likely form a defect cluster acting as a color center [9]. To confirm that the trap states do indeed have sufficiently long lifetimes, we consider the PL decay dynamics of an ensemble of CdS nanorods following an optical excitation pulse. A sample of these nanocrystals is suspended in a polystyrene block several microns thick, which is mounted to the cold finger of a closed-cycle He cryostat operating at 21 K. Pulsed optical excitation is achieved with a 355 nm diode laser and the resultant PL spectrum is captured as a function of time with a gated, intensified charge-coupled device (ICCD) camera which is mounted to a spectrometer. Figure 1a shows prompt (2 ns integration window) and delayed (10 μ s delay, 100 ns integration window) emission spectra, revealing the two distinct emissive species: the narrow blue exciton band which dominates the prompt emission; and the broad red defect band which appears at longer times. Recording the spectral decay following sub-nanosecond excitation allows confirmation of the presence of long-lived trap states [20–22] feeding these two emission channels, which have distinct lifetimes as seen in Figure 1b. Besides the requirement for long lifetimes of suitable carrier states, pODMR additionally calls for sufficient lifetimes of the spin state (i.e. T_1 should be larger than a few ns), which is also satisfied for several of the trap states existing in CdS.

For all pODMR measurements, a sample similar to the above is fabricated, with CdS nanorods dispersed within an optically inert, diamagnetic matrix. The sample is then held at

cryogenic temperatures within a He flow cryostat and a suitably damped (low-Q) dielectric Flexline resonator of a Bruker E580 pulsed EPR spectrometer. Continuous wave optical excitation is carried out with an Ar⁺ laser tuned to 457.9 nm, which is almost resonant with the band gap of CdS nanorods of this diameter (6 nm). As band-edge excitonic states are generated optically, there is some probability for them to become localized to the shallow trap states which are nearly iso-energetic with the band gap, or to lose energy and become associated with a deeper-lying chemical defect. Once charge carriers become trapped, they may either detrap and return to excitonic states; feed into nearby deep-level chemical defect states; interact with subsequent optical excitations through an Auger process; or simply thermalize to the ground state. These processes are spin dependent, so that spin manipulation in the course of pODMR experiments can be observed through transient photoluminescence experiments. In the present work we focus on the spin-dependent emission characteristics of the deep-level defect by first controlling the light emission through coherent spin excitation and then using this effect as a probe of the intermediate states involved in populating the defects and their respective environments.

Optical detection of spin resonance becomes possible by inducing a magnetic resonant spin manipulation of optically-active charge carrier pairs. Magnetic resonance is achieved by applying an external magnetic field (~ 0.34 T) to the sample and then matching the resulting Zeeman separation of its energy eigenstates with a pulsed microwave field (~ 9.8 GHz; with the frequency held constant in all measurements). The resulting resonant change in mutual spin identity for the carrier pair is then reflected by changes in PL intensity, either as an enhancement or as a quenching of the emission channel [28], as observed by acquisition from a low-noise photodiode (FEMTO LCA-S-400K-SI). In principle, individual trapping species can be fully

resolved since the resonance condition for each type is unique and corresponds to the effective Landé g -factor of that state. In order to differentiate between trap species which play a role in separate emission processes, pODMR is performed on each of the two CdS nanorod emission channels by using optical selection filters (spectral bandwidths indicated in Figure 1a). This general process of excitation, charge trapping or localization on a defect, and electron spin resonance (ESR) of optically-active carriers is schematically depicted in Figure 2a. The results of this spectrally-resolved pODMR can be seen for each emission channel in Figure 2b,d, where the resonant change in PL intensity, plotted on a color scale, is shown as a function of magnetic field strength and time following the microwave pulse. The temporally-integrated magnetic field dependence of differential PL yields the resonance spectra in Figure 2c, e.

The resonance spectrum for shallow band-edge trap states detected through the band-edge excitonic emission, shown in Figure 2c, is composed of three primary Gaussian resonances; two narrow and one broad, which all lead to PL quenching. The effects of linewidth broadening and our choice of the Gaussian lineshape have been described in our previous work on the topic [23]. It is important to note that the g -factors reported for quantum confined systems are shifted with respect to their counterparts in bulk materials, provided resonances can at all be detected. Since quantum size effects change energy level separation, spin-orbit mixing of excited and ground states is also affected by quantum confinement, leading to some deviation in g -value [29,30]. The broad central resonance ($g_2 \approx 1.96$) is likely due to a single carrier whose wavefunction is partially delocalized over the nanorod, thus experiencing a large distribution of hyperfine and strain fields. Since, in contrast to the mechanism described below, there is no indication of a pair process for resonance g_2 , we speculate that PL quenching here arises due to an Auger mechanism involving an exciton and a single trapped charge [23], in analogy to models

of blinking in single nanocrystals [11–13]. The two narrower resonances ($g_1 \approx 2.00$ and $g_3 \approx 1.85$) have been attributed to spin- $\frac{1}{2}$ carriers which are localized to the surface of the nanocrystal [23], which limits the range of magnetic environments experienced by the spins and thus the degree of environmental spectral broadening. An interesting aspect of these two narrow features is that they have the same resonance area, which describes the probability of the resonant species undergoing a spin-resonant transition followed by some form of optical activity. In addition, as shown in Figure 2f, the two peaks exhibit exactly the same time dynamics following a microwave pulse. We conclude that the two peaks must correspond to electron and hole resonances. Since the two carriers in the pair are correlated by spin-dependent recombination, the resonance of either of these two species leads to the same overall change in “bright-to-dark” exciton population ratio; once perturbed, the system evolves freely to a steady-state condition in exactly the same way at the two magnetic fields (i.e. for the two g -factors). This equality of resonant area and time dynamics makes a firm case for these carriers constituting a coupled state. It can be shown by analysis of the frequency components observed in coherent Rabi oscillations of the spin species that these signatures arise due to trapped carrier pairs experiencing negligible exchange and magnetic dipole-dipole interactions, but which are still strongly Coulombically bound [23]. Since the external magnetic field lifts the degeneracy, the mutual spin orientation in the pair assumes either singlet or triplet character, but only while these carriers remain trapped and localized. Upon detrapping to band-edge exciton states, this effective singlet-triplet character becomes projected onto the higher spin multiplicity which characterizes the excitonic fine-structure [31,32]. Therefore, changing the singlet to triplet content of trapped carrier pairs will modify the probability of moving the carrier pair back into one of the three radiative spin-allowed (“bright”) or two spin-forbidden (“dark”) exciton levels.

Ultimately, this conversion of spin multiplicity under resonance changes the overall bright-to-dark state exciton population ratio once detrapping has occurred. Similar dependencies on mutual spin orientation exist for the emissive defect center, although we note that there is no information available on the nature of its excitonic fine structure. The remainder of this work focuses on the spin-resonant dynamics observed in emission from this deep-level trap center.

The magnetic resonance spectrum detected under emission from the defect in Figure 2e exhibits four PL *enhancement* rather than quenching processes. Upon fitting the resonance structure, it is found that the same two coupled states that were observed under detection of the band-edge emission channel ($g_1 \approx 2.00$ and $g_3 \approx 1.85$) [23] are also present in resonant modulation of the defect emission, even though these are spectrally entirely distinct species. PL *quenching* of the band-edge emission under resonance correlates directly with PL *enhancement* of the defect emission. This conclusion is based not only on the equality of g -factors, but also, as before, on the identity of resonance areas and free-evolution dynamics, summarized in Figure 2f,g. Apparently, as carriers within the shallow band-edge traps (the exciton “shelving” states) are placed in a mutual spin configuration corresponding to a “dark” state, the probability of charge transfer or relaxation to the emissive defect site is increased [33]. Two important consequences are implied by this result. One is that *both* electrons and holes are transferred to the emissive defect deep-level trap, suggesting that it is actually a defect cluster which can trap both carriers. Secondly, this mechanism serves as a direct observation of a circumvention process for the phonon bottleneck problem [34] of both carrier types. The additional two resonances comprising the primary central feature in the spectrum have previously received limited attention within c.w. ODMR investigations [24]. In bulk crystalline CdS it was found that the pronounced lineshape anisotropies of multiple resonances indicate that this emissive defect is

indeed a type of donor-acceptor complex [24] which can accommodate both carriers. In contrast, in CdS nanoparticles, this resonance was purported to arise due to strong carrier-pair exchange coupling [25].

Additional information on the nature of these spin states responsible for the ODMR signal of the deep-level defect can be gained through observing coherent spin motion arising during application of powerful magnetic resonant excitation. Specifically, both spin multiplicity [35] as well as exchange [36] and dipolar [37,38] interactions leave their imprint on the frequency components of resonantly induced spin-Rabi oscillations. Transitions between different Zeeman-split m_s levels produce well-defined frequency components in the Rabi oscillations independent of the driving field amplitude, whereas components due to interactions depend on the type of interaction and vary with field strength. By sequentially driving the carriers between bright and dark state spin configurations during Rabi flopping, coherent nutation for each of the primary resonance features is demonstrated in Figure 3. Figure 3a illustrates the coherent spin propagation scheme employed. Under detection of the defect emission, PL spin Rabi flopping is shown in the inset of panel b for the two individual resonance peaks g_1 (blue, light grey) and g_3 (red, dark grey), and in the inset of panel c for the overlapping peaks g_4 and g_5 together (black). The corresponding Fourier transform of the raw data is displayed in the main figures of panels b and c with a frequency scale normalized to the free-electron-spin nutation frequency, which is given by the product of the gyromagnetic ratio ($\gamma \approx 28.024$ GHz/T) and the strength of the driving microwave field ($B_1 \approx 1$ mT). The frequency spectrum of such a decaying oscillation exhibits a swept frequency response about the primary frequency component [39]. As we reported previously, when coherent spin precession for the g_1

and g_3 resonances is read out through the band-edge emission channel [23], there is no signature of either exchange or dipolar interactions and the spin-multiplicity for each carrier is unambiguously $S = 1/2$. Surprisingly, when the same trapped carrier pairs are probed coherently, but instead information on Rabi flopping is accessed through the deep-level chemical defect emission rather than the band-edge recombination channel, a clear deviation from the previously observed [23] frequency of $\gamma\mathcal{B}_1$ is found in Fig. 3. Since the spin multiplicity of uncoupled charge carriers cannot lead to a frequency component lower than $\gamma\mathcal{B}_1$, some change in mutual spin interaction between the two carriers must have occurred. Also, an exchange interaction produces multiple frequency components [36], not a single low-frequency component as seen here. Therefore, it may be concluded that dipolar interaction has been increased for these two trap states [37,38]. This change in character is likely induced by the spatial proximity of the trap to the emissive defect cluster; the local structural environment of the surface is significantly altered by the S^{2-} and Cd^{2+} vacancies [40], thereby perturbing the more shallow trap states as well. This structural effect is witnessed by the subtle change in linewidth of a few mT for each of these resonances when going from band-edge emission detection to defect emission detection (see the Gaussian fits of the lineshapes in Figure 2f,g; for band-edge emission, widths $w_1 = 5.7$ mT and $w_2 = 8.6$ mT; for defect emission, $w_1 = 6.7$ mT and $w_2 = 5.8$ mT). By monitoring the g_1 and g_3 resonances through defect emission, we therefore probe only that subset of shallow trap states which is both spatially and energetically associated with the deep cluster defect, thereby modifying the linewidths of the resonance slightly.

The Rabi oscillations taken at the central (g_4 and g_5) resonance feature display a strong frequency component at $\gamma\mathcal{B}_1$, but also at both higher and lower frequencies. Interpreting such

information is made difficult due to the fact that the resonance structure being probed actually involves a combination of resonant features (the broad $g_5 \approx 1.93$ and the sharper $g_4 \approx 1.94$ species). Even if the frequency components of each resonance differ, they will become inseparably convoluted without higher-order measurement techniques (such as high-field EPR with control of the crystalline axis, shifting each resonance through orientation-specific crystal-field splitting). This convolution will only occur, though, for resonances where each feature experiences a sufficiently long coherence time to allow us to measure Rabi oscillations in the experiment (i.e. for $T_2 \geq 10$ ns). Consequently, determining whether convolution of the dynamics of resonance species is a factor in the transient spectroscopy requires knowledge of coherence times. If the T_2 time for each of these two resonances differ even slightly, then this should be discernible as a double-exponential decay in a Hahn spin echo experiment. Such an experiment is described below, confirming convolution of resonance species.

The conclusion that the two satellite features (g_1 and g_3) of the pair process experience dipolar coupling, as inferred from the harmonics observed in the Rabi oscillations, can be tested by the prediction of another dipolar coupling-induced resonance at approximately half-field ($g_{hf} \approx 4$). The spectrum in Figure 3d,e, recorded at half the Zeeman splitting, shows that such a resonance is indeed observed. This type of (dipole-forbidden) transition provides evidence of dipolar interactions arising from the $S = 1$ content in at least one set of the full-field transitions. In principle, the features of such a resonance can be used to help establish a rough estimate of spin-pair distances, but information on the corresponding full-field signal is also required (i.e. g -factor, lineshape anisotropy, and spin-orbit coupling tensor), which is lacking here due to the presence of multiple resonances and their respective convolution. Finally, we note that there is

no detectable half-field signal associated with the ODMR spectrum gained by monitoring the CdS band-edge emission. Strong dipolar coupling of the spin pairs can therefore only arise when these pairs are associated with emission from the deep-level defect, implying that in such species trapped electron and hole states are spatially strongly correlated.

In order to gain insight into the nature of spin relaxation of the resonance about $g = 1.94$ we use the Hahn spin-echo pulse sequence as outlined schematically in Figure 4a. In conventional pulsed EPR experiments, the Hahn-echo sequence is employed as a two-pulse series consisting of an initialization and an inversion pulse. For the purpose of pODMR Hahn-echoes, we have extended this technique by a third pulse, a spin-projection (readout) pulse. Since ODMR spectroscopy probes spin permutation symmetry states rather than spin polarization (as in conventional ESR), this adaptation places the configuration of the rephasing spin ensemble back into an observable state (i.e. an optically bright or dark mutual spin configuration).

The results of this measurement procedure confirm that two long-coherence states are indeed probed at the broad resonance about $g = 1.94$ (i.e. g_4 and g_5), leading to an observed double-exponential decay of the echo magnitude as a function of inter-pulse delay time as shown in Fig. 4b. Remarkably, the coherence of the longer-lived spin species persists into the microsecond timescale. Such long coherence times are reminiscent of diamond nitrogen-vacancy centers. Even in diamond, coupling to nearby defects [41] can cause charge fluctuations [42] and spin dephasing. Such processes also likely occur here. Nevertheless, this particularly long-lived spin state in semiconductor nanocrystals could find utility in quantum information processing and quantum-enhanced sensing schemes [43]. We note that correlating each of the two coherence time components in the measured composite spin echo decay to a respective magnetic resonance could be made possible with selective resonance detection using electron spin-echoes observed

beyond the shorter coherence lifetimes, i.e. by temporally gating out the shortest-lived component.

Additional information on the immediate chemical environment of the spin state can be gained from the long-lived spin coherence. The pronounced modulation present in the echo decay envelope in Figure 4b arises due to interactions between the spin of a trapped carrier and its local environment. Such an effect is referred to as electron spin-echo envelope modulation, or ESEEM [44,45]. Figure 4c shows the pure contribution of the echo signal due to ESEEM, with the biexponential echo decay removed. The corresponding Fourier transform of the ESEEM oscillations are given in panel d for illustration purposes. In the present case, where a strong ESEEM component is observed at about 1.8 MHz, we conclude that ESEEM arises due to either hyperfine coupling with cadmium nuclear magnetic moments or from dipolar coupling with a nearby carrier. Differentiation between these two cases is at present complicated due to the ambiguity of dipolar and hyperfine interaction strengths. Nonetheless, the modulation of the echo signal demonstrates the potential of using long-coherence states in colloidal nanocrystals as a local probe of the defect's exact chemical environment.

In this study, we have shown how pODMR can be used as a probe of the nature and environment of distinct charge trap and emissive chemical defect states in CdS nanorods. Particular attention has been paid to describing the spin-resonant dynamics involved in the deep-level chemical defect emission common to CdS nanocrystals. It was found that shallow trap states which interact with band-edge excitons also provide a relaxation channel to the lower-lying emissive defect state. However, only those band-edge states which control emission through the low-energy defect states show significant dipolar coupling, which is detectable both through the full magnetic field Rabi oscillations as well as the half-field resonance. This

coupling indicates that the states within these band-edge carrier pairs are of much closer proximity than the states which lead to band-edge recombination, where no dipolar coupling is identified. Hahn spin-echo measurements detected in the emission of the defect itself expose an extraordinarily long spin coherence lifetime. At $T_2 \approx 1.6 \mu\text{s}$ at 3.5 K, this value is surprisingly high for colloidal nanocrystals, even compared to magnetically-doped particles [44]. In addition, the ESEEM signal can provide valuable chemical and structural insight needed in order to engineer this well-known [14] yet incompletely characterized emissive defect out of the CdS nanocrystal synthesis process. Finally, we note the astonishing likeness between some of the spin-dependent photophysics of semiconductor nanocrystals reported here and previously [23] and spin-coherence phenomena in organic semiconductors, in particular relating to the $g_1 \approx 2.00$ resonance and the extraordinary spin coherence time seen in spin echo measurements [46]. This similarity likely relates to the clear correspondence in magnetoresistance and magnetoluminescence experiments between films of organic semiconductors [47] and inorganic nanocrystals [48], which in turn can be attributed to hyperfine-field-mediated pair processes.

Acknowledgements

Acknowledgment is made to the Department of Energy Grant (#DESC0000909) for funding of this research. This material presented is based upon work supported by the National Science Foundation under Grant No. DMR 11-21252. J.M.L. and D.V.T. are indebted to the David and Lucile Packard Foundation for providing fellowships. C.B. and D.V.T. acknowledge support by National Science Foundation CAREER grants (#0953225 and #0847535, respectively).

References:

- [1] O. E. Semonin, J. M. Luther, S. Choi, H.-Y. Chen, J. Gao, A. J. Nozik, and M. C. Beard, *Science* **334**, 1530–1533 (2011).
- [2] C. Dang, J. Lee, C. Breen, J. S. Steckel, S. Coe-Sullivan, and A. Nurmikko, *Nat. Nanotech.* **7**, 335–339 (2012).
- [3] V. Wood, M. J. Panzer, J. Chen, M. S. Bradley, J. E. Halpert, M. G. Bawendi, and V. Bulović, *Adv. Mater.* **21**, 2151–2155 (2009).
- [4] J. Tang, K. W. Kemp, S. Hoogland, K. S. Jeong, H. Liu, L. Levina, M. Furukawa, X. Wang, R. Debnath, D. Cha, K. W. Chou, A. Fischer, A. Amassian, J. B. Asbury, and E. H. Sargent, *Nat. Mater.* **10**, 765–771 (2011).
- [5] D. Zhitomirsky, I. J. Kramer, A. J. Labelle, A. Fischer, R. Debnath, J. Pan, O. M. Bakr, and E. H. Sargent, *Nano. Lett.* **12**, 1007–1012 (2012).
- [6] F. M. Gómez-Campos and M. Califano, *Nano Lett.* **12**, 4508–4517 (2012).
- [7] S. A. Fischer, A. M. Crotty, S. V Kilina, S. A. Ivanov, and S. Tretiak, *Nanoscale* **4**, 904–914 (2012).
- [8] O. Voznyy, *J. Phys. Chem. C* **115**, 15927–15932 (2011).
- [9] N. Chestnoy, T. D. Harris, R. Hull, and L. E. Brus, *J. Phys. Chem.* **90**, 3393–3399 (1986).
- [10] D. V. Bavykin, E. N. Savinov, and V. N. Parmon, *Langmuir* **15**, 4722–4727 (1999).
- [11] J. Zhao, G. Nair, B. R. Fisher, and M. G. Bawendi, *Phys. Rev. Lett.* **104**, 157403 (2010).
- [12] S. Rosen, O. Schwartz, and D. Oron, *Phys. Rev. Lett.* **104**, 157404 (2010).
- [13] C. Galland, Y. Ghosh, A. Steinbrück, M. Sykora, J. a. Hollingsworth, V. I. Klimov, and H. Htoon, *Nature* **479**, 203–207 (2011).
- [14] A. Vuylsteke and Y. Sihvonen, *Phys. Rev.* **113**, 40–42 (1959).
- [15] Y. Wang and N. Herron, *J. Phys. Chem.* **92**, 4988–4994 (1988).
- [16] P. Neřmec and P. Malý, *J. Appl. Phys.* **87**, 3342–3348 (2000).
- [17] D. V Talapin, J. H. Nelson, E. V Shevchenko, S. Aloni, B. Sadtler, and A. P. Alivisatos, *Nano Lett.* **7**, 2951–2959 (2007).

- [18] A. L. Efros and M. Rosen, *Phys. Rev. Lett.* **78**, 1110–1113 (1997).
- [19] P. A. Frantsuzov and R. A. Marcus, *Phys. Rev. B* **72**, 155321 (2005).
- [20] A. F. van Driel, I. S. Nikolaev, P. Vergeer, P. Lodahl, D. Vanmaekelbergh, and W. L. Vos, *Phys. Rev. B* **75**, 035329 (2007).
- [21] M. Jones, S. S. Lo, and G. D. Scholes, *Proc. Natl. Acad. Sci.* **106**, 3011–3016 (2009).
- [22] M. Jones, S. S. Lo, and G. D. Scholes, *J. Phys. Chem. C* **113**, 18632–18642 (2009).
- [23] K. J. van Schooten, J. Huang, W. J. Baker, D. V. Talapin, C. Boehme, and J. M. Lupton, *Nano Lett.* **13**, 65–71 (2013).
- [24] A. Edgar and J. Pörsch, *Solid State Commun.* **44**, 741–743 (1982).
- [25] E. Lifshitz, I. D. Litvin, H. Porteanu, and A. A. Lipovskii, *Chem. Phys. Lett.* **295**, 249–256 (1998).
- [26] S.-Y. Paik, S.-Y. Lee, W. J. Baker, D. R. McCamey, and C. Boehme, *Phys. Rev. B* **81**, 075214 (2010).
- [27] R. M. Kraus, P. G. Lagoudakis, A. L. Rogach, D. V. Talapin, H. Weller, J. M. Lupton, and J. Feldmann, *Phys. Rev. Lett.* **98**, 017401 (2007).
- [28] D. R. McCamey, S.-Y. Lee, S.-Y. Paik, J. M. Lupton, and C. Boehme, *Phys. Rev. B* **82**, 125206 (2010).
- [29] J. A. Gupta, D. D. Awschalom, A. L. Efros, and A. V. Rodina, *Phys. Rev. B* **66**, 125307 (2002).
- [30] P. G. Baranov, S. B. Orlinskii, D. M. Hofmann, C. D. M. Donegá, A. Meijerink, and J. Schmidt, *Phys. Status Solidi B* **247**, 1476–1479 (2010).
- [31] A. Efros, M. Rosen, M. Kuno, M. Nirmal, D. Norris, and M. Bawendi, *Phys. Rev. B* **54**, 4843–4856 (1996).
- [32] P. Horodyská, P. Němec, D. Sprinzl, P. Malý, V. N. Gladilin, and J. T. Devreese, *Phys. Rev. B* **81**, 045301 (2010).
- [33] J. Davies, *J. Phys. C: Solid State Phys.* **16**, L867–L871 (1983).
- [34] D. Schroeter, D. Griffiths, and P. Sercel, *Phys. Rev. B* **54**, 1486–1489 (1996).
- [35] A. V. Astashkin and A. Schweiger, *Chem. Phys. Lett.* **174**, 595–602 (1990).

- [36] A. Gliesche, C. Michel, V. Rajevac, K. Lips, S. D. Baranovskii, F. Gebhard, and C. Boehme, *Phys. Rev. B* **77**, 245206 (2008).
- [37] M. E. Limes, J. Wang, W. J. Baker, S.-Y. Lee, B. Saam, and C. Boehme, arXiv:1210.0950 (2012).
- [38] R. Glenn, M. E. Limes, B. Saam, C. Boehme, and M. E. Raikh, arXiv:1210.0948 (2012).
- [39] R. Glenn, W. J. Baker, C. Boehme, and M. E. Raikh, arXiv:1207.1754 (2012).
- [40] Y. R. Wang and C. B. Duke, *Phys. Rev. B* **37**, 6417–6424 (1988).
- [41] B. Naydenov, F. Reinhard, A. Lammle, V. Richter, R. Kalish, U. F. S. D’Haenens-Johansson, M. Newton, F. Jelezko, and J. Wrachtrup, *Appl. Phys. Lett.* **97**, 242511 (2010).
- [42] L. Rondin, G. Dantelle, A. Slablab, F. Grosshans, F. Treussart, P. Bergonzo, S. Perruchas, T. Gacoin, M. Chaigneau, H.-C. Chang, V. Jacques, and J.-F. Roch, *Phys. Rev. B* **82**, 115449 (2010).
- [43] J. R. Weber, W. F. Koehl, J. B. Varley, A. Janotti, B. B. Buckley, C. G. Van de Walle, and D. D. Awschalom, *Proc. Natl. Acad. Sci.* **107**, 8513–8518 (2010).
- [44] S. T. Ochsenbein and D. R. Gamelin, *Nat. Nanotech.* **6**, 112–115 (2011).
- [45] F. Hoehne, J. Lu, A. Stegner, M. Stutzmann, M. Brandt, M. Rohrmüller, W. Schmidt, and U. Gerstmann, *Phys. Rev. Lett.* **106**, 196101 (2011).
- [46] W. J. Baker, T. L. Keevers, J. M. Lupton, D. R. McCamey, and C. Boehme, *Phys. Rev. Lett.* **108**, 267601 (2012).
- [47] M. Reufer, M. J. Walter, P. G. Lagoudakis, A. B. Hummel, J. S. Kolb, H. G. Roskos, U. Scherf, and J. M. Lupton, *Nat. Mater.* **4**, 340–346 (2005).
- [48] A. Pourret, A. Ramirez, and P. Guyot-Sionnest, *Appl. Phys. Lett.* **95**, 142105 (2009).

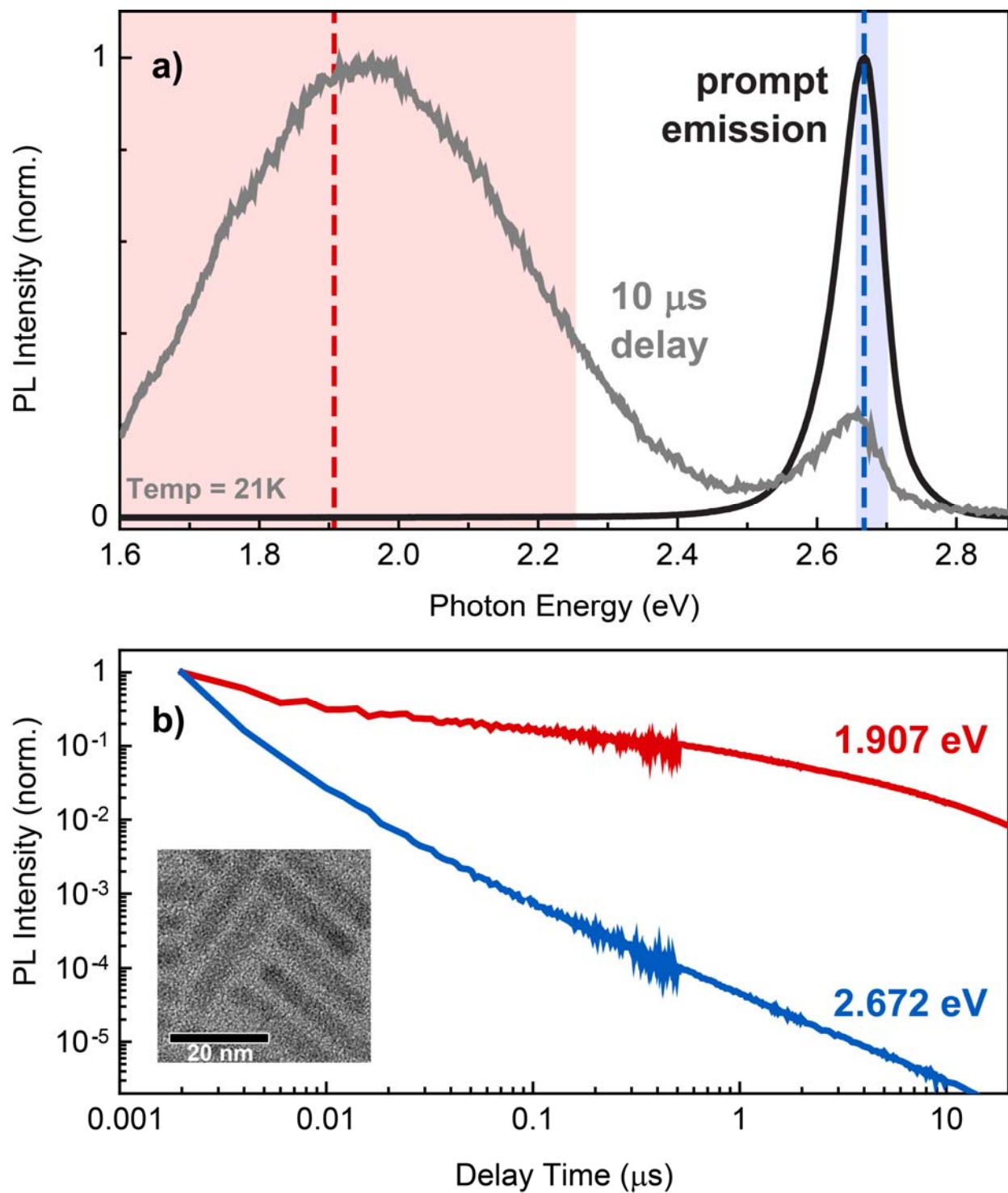


Figure 1. (Color online) Time-resolved luminescence of CdS nanorods exhibiting long-lived dual emission fed by trap states. (a) Prompt (0-2 ns integration window) and 10 μs delayed (10-10.1 μs integration window) optical emission spectra of nanorods confined in a thin polymer matrix film,

following 0.7 ns pulsed excitation from a 355 nm diode laser at 21 K. Prompt emission is dominated by band-edge exciton recombination, whereas the broad, red luminescence channel appearing at longer delay times is attributed to deep-level chemical defect states. The light blue (light grey) and red (dark grey) regions denote the spectral bandwidth of collection filters used for luminescence channel isolation in the pODMR experiments. Vertical blue and red dashed lines mark the spectral positions used to demonstrate the existence of long-lived trap states feeding each emission channel, as is evident by the long power-law-like PL decays given in panel (b). The detection gate integration window of the ICCD used for each step in time delay was: 2 ns for 0-510 ns; 20 ns for 0.51-2.0 μ s; 100 ns for 2.0-10 μ s; 1.0 μ s for 10-20 μ s. The inset shows a transmission electron micrograph illustrating the high quality of CdS nanocrystalline nanorods.

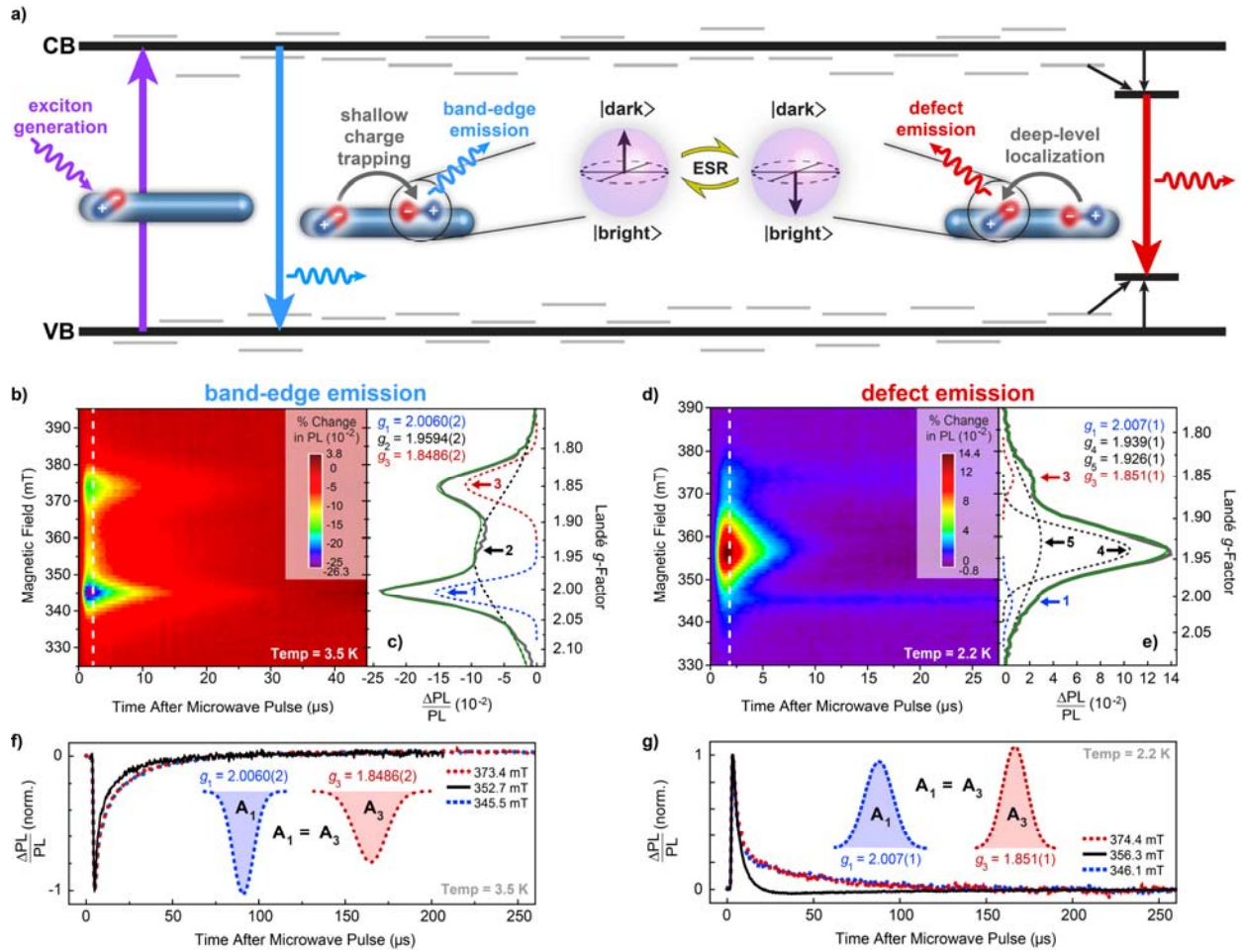


Figure 2. (Color online) Correlating trap states with spectrally-dependent ODMR. a) Optical excitation near the band edge populates the lowest exciton state. This exciton either recombines radiatively, localizes to shallow trap states (light grey lines), or dissipates to the chemical defect (thick black lines inside CB and VB). Long carrier trapping lifetimes allow for use of ESR in changing the mutual spin configuration of trapped charge pairs, modulating optically “bright” and “dark” population ratios and thereby affecting the resultant PL intensity from each of the two emission channels. (b) Spin resonance mapping and (c) resonance spectrum for shallow trap states affecting band-edge exciton emission; and (d), (e) the same for defect emission. Multiple resonances (i.e. optically-active carrier states) are observed through each emission channel. Two resonances ($g_1 \approx 2.00$ and $g_3 \approx 1.85$) are found to be common to both emission channels, indicating that both band-edge excitons and emissive chemical defects interact

with the same species of shallow band-edge trap states. (f), (g) These two resonances arise due to a coupled carrier pair (i.e. electron and hole), as evidenced by the correlations in resonance peak areas and temporal dynamics for each emission channel. The dynamics of the broad resonance g_2 (band-edge emission, black line in f) and the superimposed resonances g_4 and g_5 (defect emission, black line in g) differ from those of the respective carrier pairs (resonances g_1 and g_3 , blue and red / dark grey dotted lines, respectively). Data were acquired under steady-state optical excitation after application of a single microwave pulse of approximately 800 ns duration. The quoted precision of the g -factors arises from the Gaussian fit to the resonance line shape.

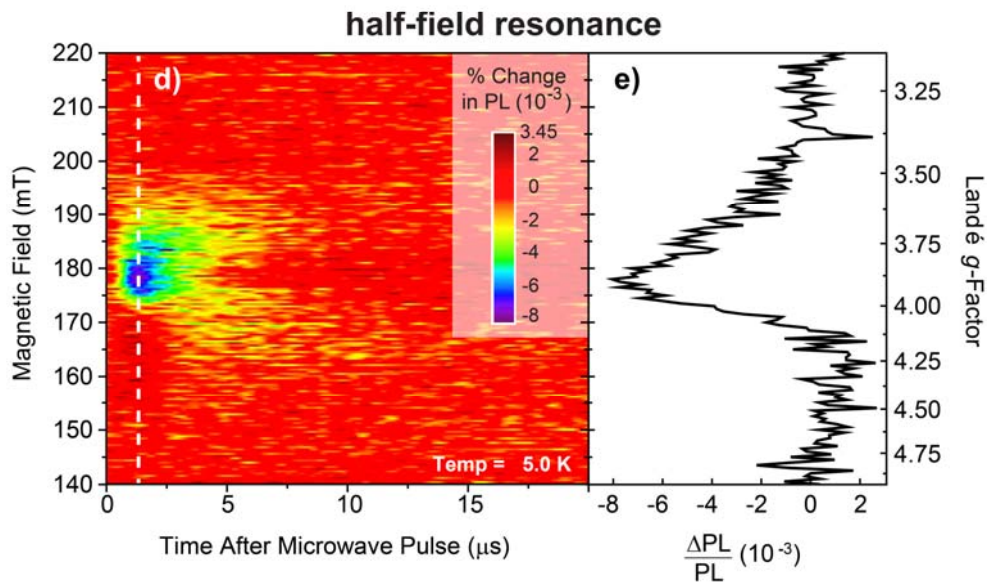
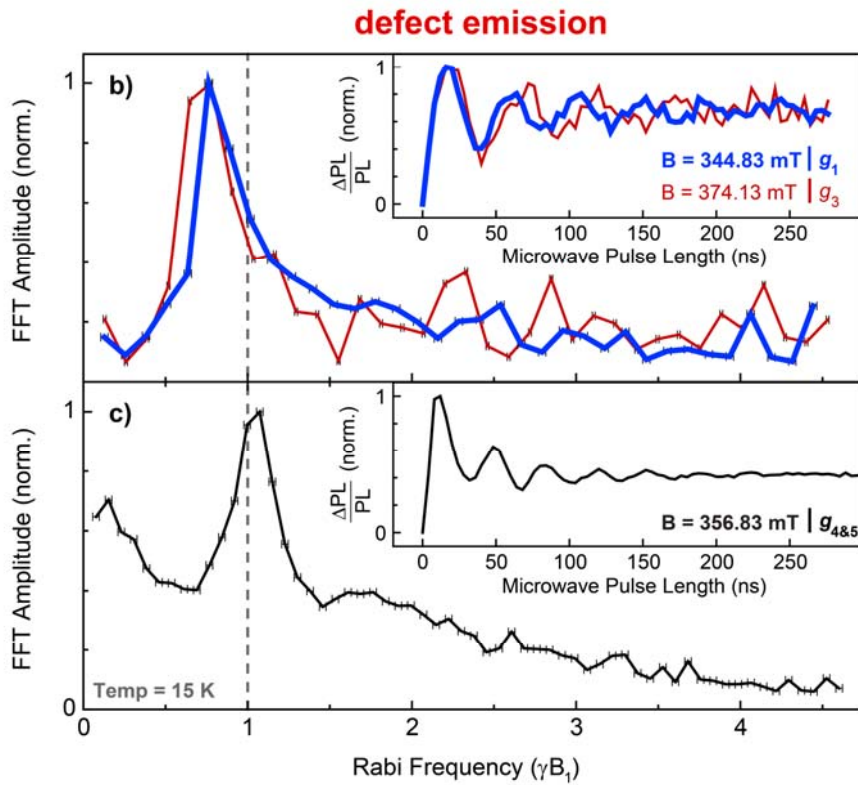
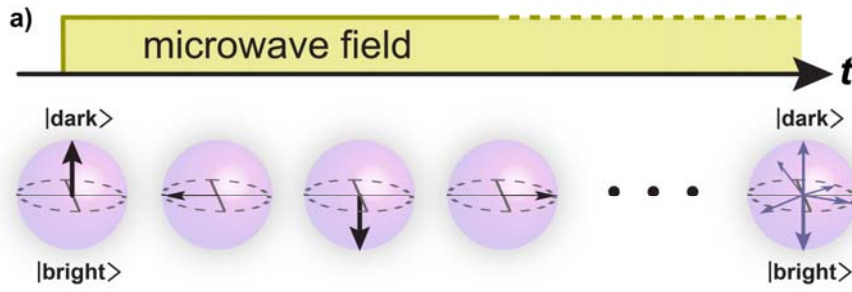


Figure 3. (Color online) Rabi oscillations as a probe of carrier interactions, detected in the low-energy defect emission: evidence for dipolar coupling. (a) Coherent Rabi oscillations are driven by a microwave field, which reversibly nutates the spin pair between optically bright and dark mutual spin configurations, enabling read-out of the spin state through the emission intensity. (b), (c) Fourier transform of the Rabi oscillations of the emissive defect resonances g_1 and g_3 [as identified in Fig. 2(d)]; and of the convoluted resonances g_4 and g_5 . The insets show the measured Rabi oscillations in the time domain. The frequency components observed in panel (b) indicate the occurrence of dipolar coupling, while those in (c) are difficult to assign due to the convolution of multiple resonances. (d) The half-field resonance confirms the existence of dipolar coupling for at least one of the full-field signals.

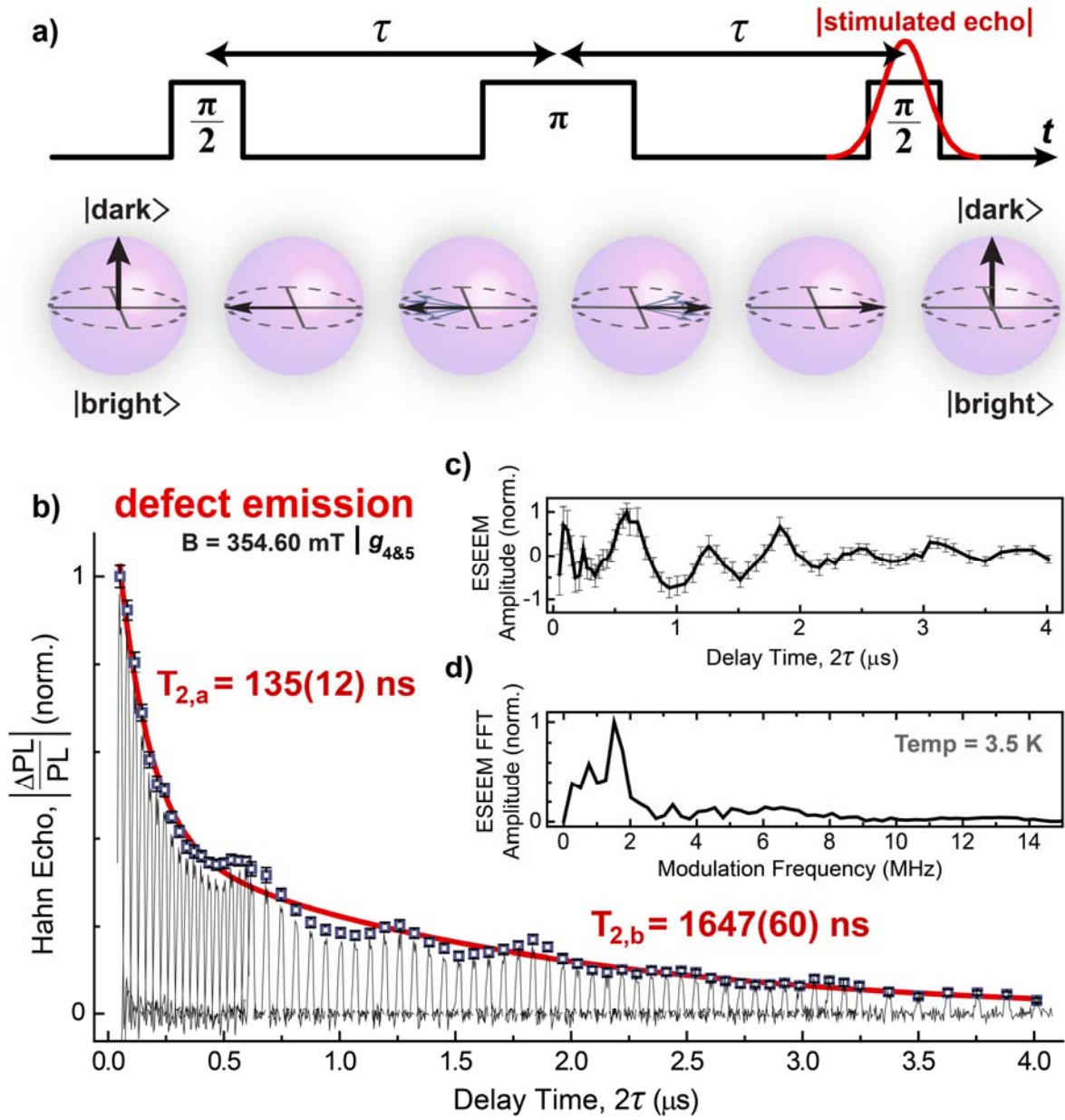


Figure 4. (Color online) Hahn spin echoes revealing slow dephasing, detected in the low-energy defect PL. (a) The conventional Hahn echo pulse sequence is modified for pODMR in order to place the remaining state polarization into an optically observable state. (b) The decay of the spin echo recorded in defect emission for the center resonance feature [convolution of peaks g_4 and g_5 , as labeled in Fig. 2(d)] is biexponential, suggesting the involvement of two independently resonant carriers under the same resonance condition, but with distinct dephasing pathways. The very long coherence time of one of these

carriers in effect allows probing of the corresponding chemical environment, leading to an electron spin-echo envelope modulation (ESEEM) of the signal. (c) ESEEM signal with the biexponential decay removed, and (d) corresponding Fourier transform.